Supplementary Materials for

Confined necking and improved tensile ductility in heterostructured bi-metallic steels made by additive manufacturing

Xiao Shang[1], Chenwei Shao[1], Soumya S. Dash[1], LuLu Guo[1], Joseph Agyapong[2], Lizhong Lang[1], Alec Chen[1], Sang Bum Yi[1], Tianyi Lyu[1], Hao Chen[1], Solomon Boakye-Yiadom[2], and Yu Zou[1]*

[1] Department of Materials Science and Engineering, University of Toronto, Toronto, ON, Canada, M5S 3E4

[2] Department of Mechanical Engineering, York University, Toronto, ON, Canada, M3J 1P3

*Corresponding author. Email: mse.zou@utoronto.ca

This file includes:

Figures. S1 to S6
Tables S1 and S2

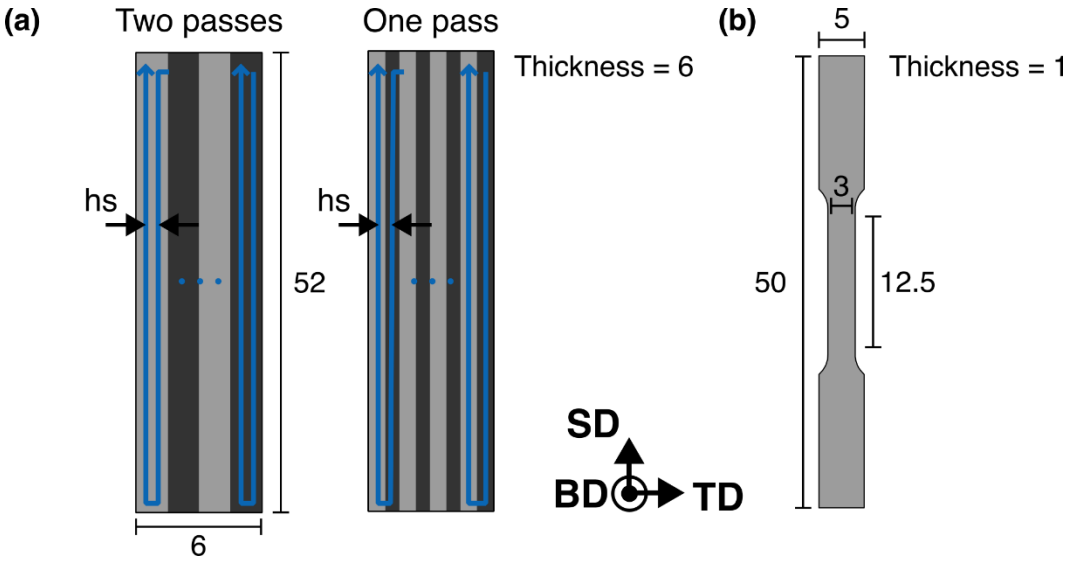

Figure S1. Tensile coupon dimensions and printing paths. (a) Schematics showing the dimensions of two as-fabricated cuboids, as well as two corresponding printing paths. For given sets of process parameters, the printing strategy with two passes results in thicker lamellae. **(b)** Schematic showing the dimensions of the tested tensile coupons. All units are in mm. The coordinates, i.e., build direction (BD), scan direction (SD), and transverse direction (TD) are labelled.

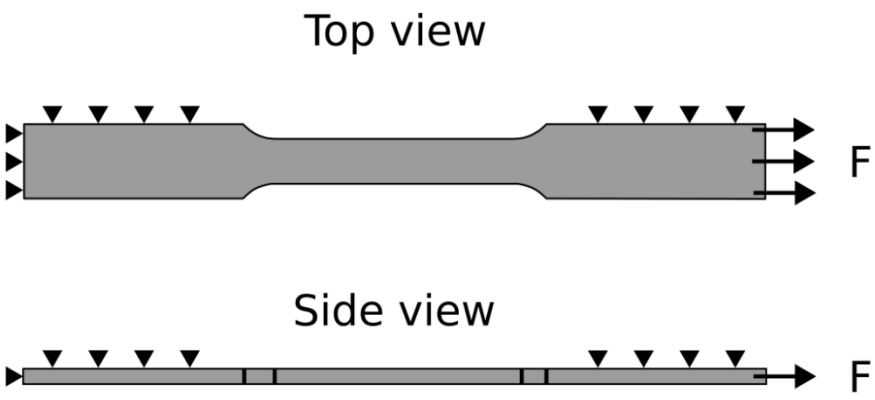

Figure S2. Boundary conditions for the FEA simulations.

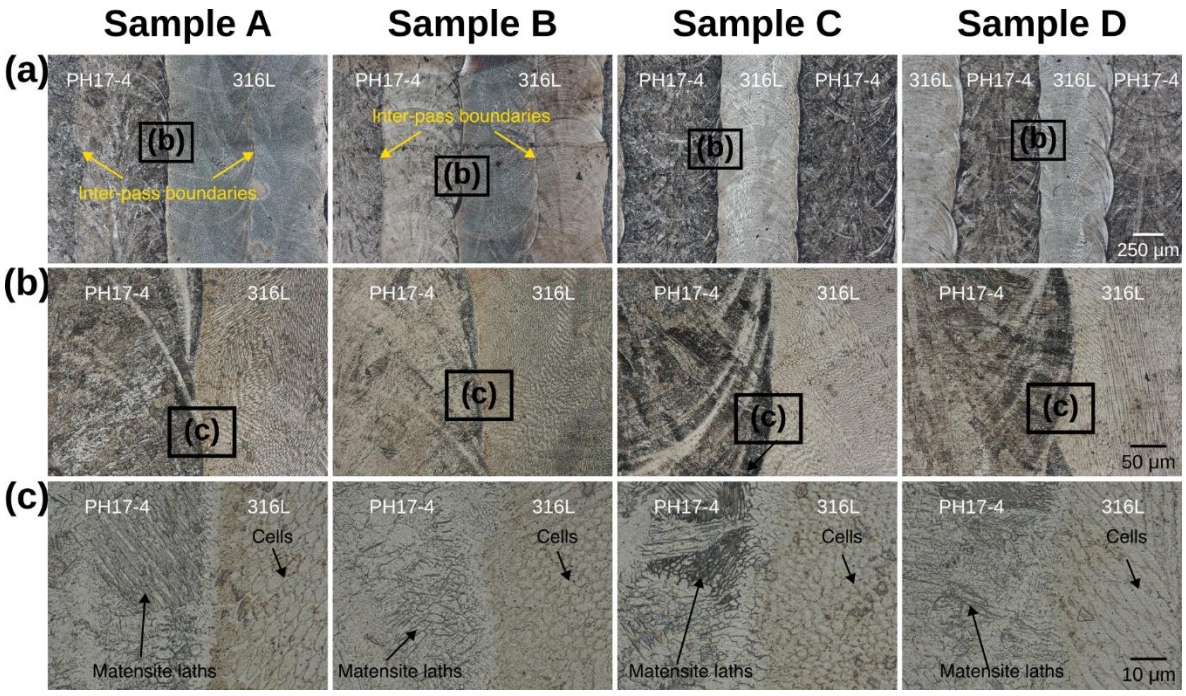

Figure S3. Microstructure of the four heterostructured designs under an optical microscope using (a) low, (b) medium, and (c) high magnifications.

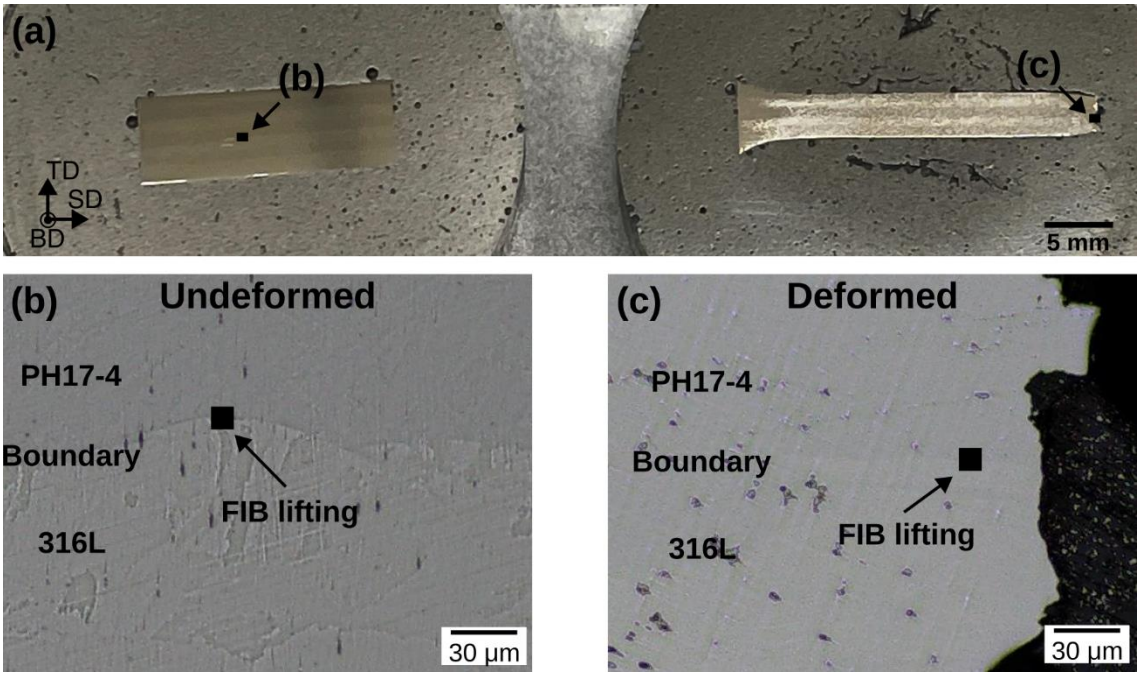

Figure S4. FIB lifting areas in deformed and undeformed samples. (**a**) Optical microscope (OM) image of the undeformed (left) and deformed (right) samples. (**b**) and (**c**) High magnification OM images on the undeformed and deformed samples, respectively. The FIB lifting regions are marked.

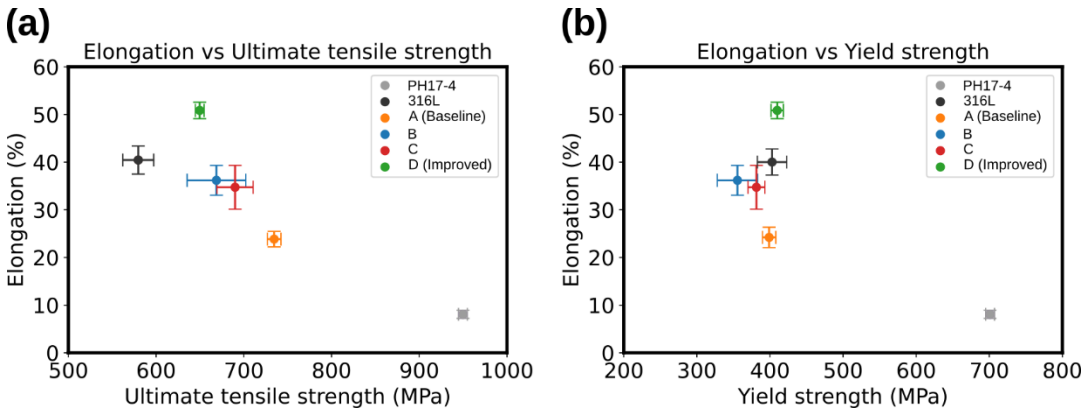

Figure S5. Derived tensile properties for each sample with error bar. (**a**) Elongation at break and ultimate tensile strength. (**b**) Elongation at break and yield strength.

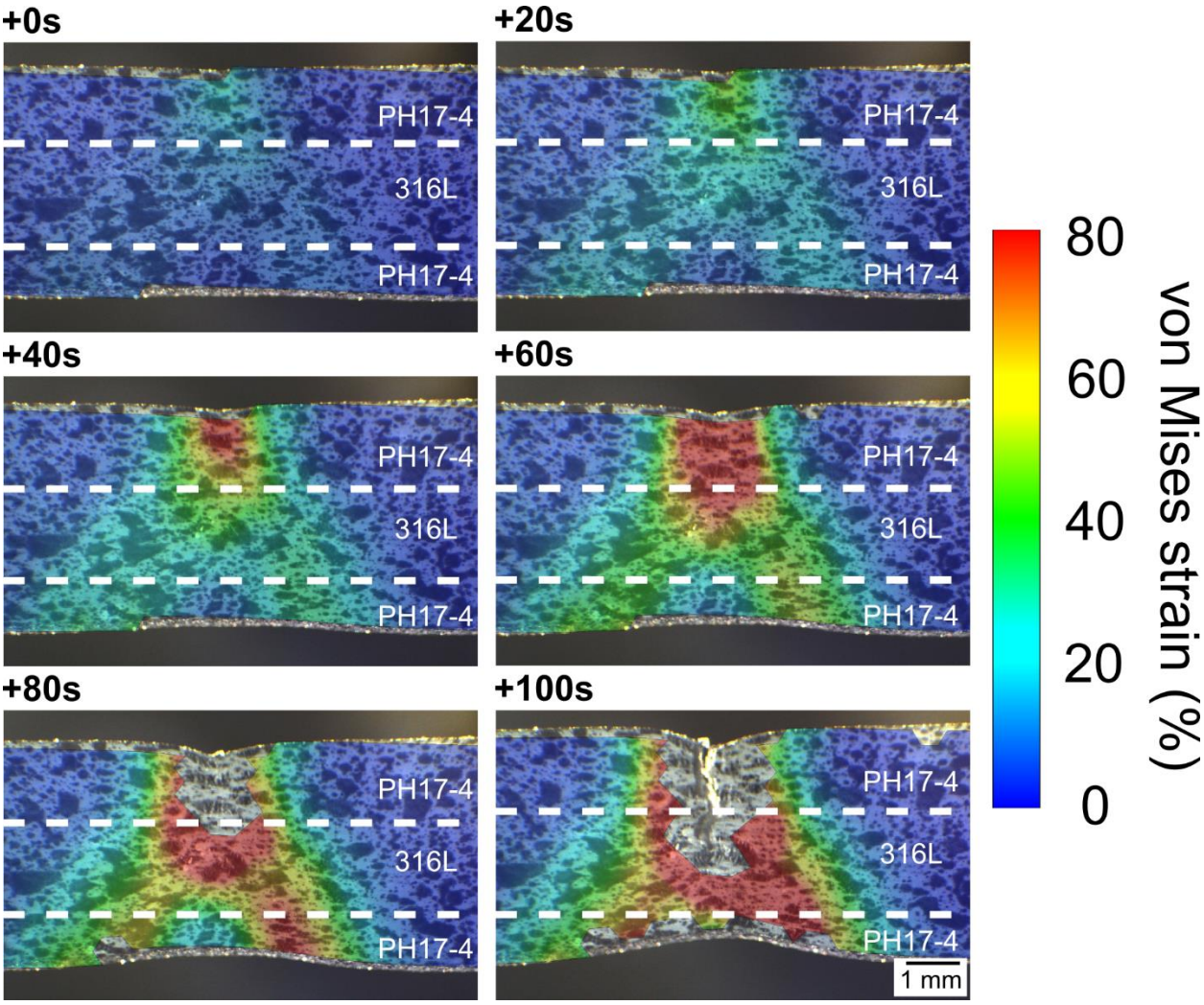

Figure S6. Von Mises strain fields of sample B at various timestamps during the tensile test, illustrating strain evolution in confined-necking co-deformation. Regions of PH17-4 and 316L are labelled.

Table S1. Process parameters for sample fabrication

Samples	Laser power (P), W	Scan speed (v), mm/s	Powder feed rate ($\dot{m}$), g/min	Hatch spacing (hs), mm	Number of passes before powder switching (np)
PH17-4	450	4	0.175	0.70	NA
316L	450	4	0.175	0.70	NA
A (Baseline)	450	4	0.175	0.81	2
B	450	4	0.175	0.70	2
C	450	4	0.175	0.81	1
D (Improved)	450	4	0.175	0.70	1

Table S2. Measured versus rule of mixture (ROM) calculated mechanical properties for samples tested in this work

Samples	*UTS (MPa)*	*UTS-ROM (MPa)*	*YS (MPa)*	*YS-ROM (MPa)*	*E (GPa)*	*E-ROM (GPa)*
316L	582.8±18.51	NA	402.8±20.28	NA	129.2±17.29	NA
PH17-4	949.8±5.24	NA	701.1±5.05	NA	130.1±3.13	NA
A (Baseline)	734.6±7.75	757.1	398.9±9.10	544.5	123.4±13.46	129.6
B	668.8±33.43	794.2	355.5±27.62	574.6	132.1±17.53	129.7
C	690.0±20.60	756.8	381.5±11.51	544.2	136.7±16.58	129.6
D (Improved)	649.7±4.99	792.0	409.9±8.44	572.8	138.6±5.92	129.7

In general, the simple rule of mixture (ROM) calculation tends to overestimate ultimate tensile strength (UTS) and yield strength (YS), while accurately capturing Young's modulus (E). This suggests that the ROM cannot be applied in the heterostructured steels (HS) for estimating the mechanical properties after the elastic regime, since deformation mechanisms not seen in conventional homogenous materials dominate the plastic deformation of the HS. During a tensile test, as soon as the 316L portion yields, the stress increase rate on the 316L portion decreases drastically. At the same time, the stress on the PH17-4 portion continues to increase at a high rate up to PH17-4's yield point, when the HS sample yields globally. When the global YS of the sample is calculated, despite the higher stress on the PH17-4 portion, the YS value is diluted by the cross-section area of both 316L and PH17-4, making it lower than that of the ROM calculated value. In terms of the UTS, as discussed in the main text of this article, the deformation of the HS near and after the necking tendence of the PH17-4 portion is governed by new mechanisms such as the confined-necking co-deformation, making the ROM inapplicable.

The results in **Table S2** also reveal that HSs with similar material volume fractions can show very different mechanical properties (i.e., samples A and C, B and D), highlighting the importance of internal heterogeneity, i.e., the lamella width, the arrangement of the lamellae, and the number of interfaces.